Journal of Geophysical Research: Earth Surface

RESEARCH ARTICLE
10.1029/2017JF004560

On Bedload and Suspended Load Measurement Performances in Sheet Flows Using Acoustic and Conductivity Profilers

G. Fromant[1], R. S. Mieras[2,3], T. Revil-Baudard[1], J. A. Puleo[2], D. Hurther[1], and J. Chauchat[1]

[1]Laboratory of Geophysical and Industrial Flow (LEGI), CNRS - Grenoble-INP - UGA, Grenoble, France, [2]Center for Applied Coastal Research, Civil and Environmental Engineering, University of Delaware, Newark, DE, USA, [3]Marine Geosciences Division, U.S. Naval Research Laboratory U.S. Naval Research Laboratory, Marine Geosciences Division, Stennis Space Center, MS, USA

Key Points:
- A comparative analysis of acoustic and conductivity-based measurements was done under sheet flow conditions with two acrylic particle sizes
- CCP and nonintrusive ACVP concentrations were measured across the dilute suspension and sheet layer with relative errors of less than 10%
- Different ACVP and CCP bed detection methods to estimate the sheet layer thickness agree within two to three particle diameters

Supporting Information:
- Supporting Information S1

Correspondence to:
G. Fromant,
guillaume.fromant@univ-grenoble-alpes.fr

Citation:
Fromant, G., Mieras, R. S., Revil-Baudard, T., Puleo, J. A., Hurther, D., & Chauchat, J. (2018). On bedload and suspended load measurement performances in sheet flows using acoustic and conductivity profilers. *Journal of Geophysical Research: Earth Surface*, *123*. https://doi.org/10.1029/2017JF004560

Received 16 NOV 2017
Accepted 19 SEP 2018
Accepted article online 21 SEP 2018

Abstract Intense sediment transport experiments were performed in a gravity-driven open-channel flow with two sizes of uniformly distributed nonspherical acrylic particles having median diameters of 1.0 and 3.0 mm and a maximum packing volumetric concentration (ϕ) of 0.55. The flow conditions were adapted to each particle size to ensure similar sediment transport flow regimes as sheet flow corresponding to Shields numbers slightly above unity and a suspension number, ratio of settling velocity to friction velocity, near unity for the two experiments. An acoustic scattering-based system (Acoustic Concentration and Velocity Profiler) and conductivity probes (Conductivity Concentration Profiler [CCP]) with two different vertical resolutions, 1 mm (CCP_{1mm}) and 2 mm (CCP_{2mm}) were used to measure instantaneous concentration profiles across the bedload and suspension layers. Measured concentration profiles, bed interface position, and sheet flow layer thicknesses are compared between the two techniques. The capabilities and limitations of both technologies are outlined. Average volumetric sediment concentration profiles were overestimated by 10% with the Acoustic Concentration and Velocity Profiler in the dense sheet layer when $\langle\phi(z)\rangle \gtrsim 0.35$, and by 100% with the CCP in the more diluted region when $\langle\phi(z)\rangle \lesssim 0.015$ and $\langle\phi(z)\rangle \lesssim 0.20$ for CCP_{1mm} and CCP_{2mm}, respectively. Good agreement is found between the three systems in terms of average and time-resolved bed level position and sheet layer thickness, validating the different bed interface detection methods on data from the two sensors.

1. Introduction

Over the past two decades, considerable research efforts have been dedicated to the understanding and modeling of sediment transport processes under energetic flow forcing conditions for which bedload moves as a sheet flow. In this context, it is widely accepted that the geophysical community suffers from a technological lack of high-resolution flow measurement tools adapted to the study of sediment transport physics in environmental flows (Liu et al., 2016; Roelvink & Brøker, 1993). Whether the sediment transport is driven by gravity, density, tidal currents, surface waves, or internal waves in river, estuarine, or coastal flows, the ability to profile sediment transport across the entire bottom boundary layer over a mobile sediment bed is currently limited to a few measurement technologies. The limited measurement capabilities has limited advances in process-based modeling of sediment transport in contrast to empirical models commonly implemented in numerical engineering codes applied for long-term predictions of morphological evolution. Such predictions are known to be subject to large uncertainties and errors which is a main research concern in the context of adaptation to abrupt climate changes.

In the past decades, two-phase flow modeling has been developed to account for the dynamic interactions between fluid and solid phases (Berzi, 2011; Chiodi et al., 2014; Hsu et al., 2003; Jackson, 1997; Jenkins & Hanes, 1998; Liu et al., 2016; Revil-Baudard & Chauchat, 2013). This approach considers the detailed fluid momentum and sediment concentration mixing processes occurring in the sheet flow layer, dominated by particle-particle interactions, up to the turbulence-driven dilute suspension layer. The theoretical modeling framework includes all possible fluid-particle interaction mechanisms; however, validation and optimization require advanced high-resolution measurement tools capable of sediment flux profiling (as the product of concentration and velocity profiles) at turbulent flow scales across both the suspension and sheet flow layers.

High particle concentration ($0.08 < \phi < 0.55$, where ϕ is volumetric concentration) and limited vertical thickness (of the order of 10–100 particle size) of the sheet flow layer makes it particularly difficult to accurately measure the particle velocities and concentrations with conventional nonintrusive optical and

acoustic flow measuring tools. The difficulty is mainly because light and sound propagation are subject to strong scattering-dominated attenuation. Only few data sets of high-resolution sheet flow measurements are available. Time-averaged volumetric concentration and velocity profiles were measured in small-scale pipe flow experiments using gamma-ray and conductivity techniques, respectively (Daniel, 1965; Horikawa et al., 1982; Nnadi & Wilson, 1992; Pugh & Wilson, 1999; Wilson, 1966). Novel techniques were developed later, aimed at measuring local concentration and streamwise velocity measurements involving the use of pointwise capacitance probes (Horikawa et al., 1982; Ribberink & Al-Salem, 1994; Sumer et al., 1996), borescopic techniques (Cowen et al., 2010), two-component particle velocity and mean concentration profiles through video imaging (Armanini et al., 2005; Capart & Fraccarollo, 2011; Spinewine et al., 2011). and pointwise intrusive conductivity meters with automated bed level tracking capability (van der Zanden et al., 2015; van der Zanden et al., 2017). Only recently have advanced acoustic and conductivity techniques been developed (Lanckriet et al., 2013; Mieras et al., 2017) and used (Hurther & Thorne, 2011; Mieras et al., 2017; Naqshband, Ribberink, Hurther, Barraud, et al., 2014; Naqshband, Ribberink, Hurther, & Hulscher, 2014; Puleo et al., 2016, 2014; Revil-Baudard et al., 2015) to profile such challenging media at sufficiently high temporal (O(0.1 s)) and spatial (O(0.001 m)) resolutions to actually measure the multiscale benthic boundary layer sediment transport processes.

This paper reports on detailed measurements of particle concentration and velocity profiles under shear-driven sheet flow transport conditions involving two fundamentally different measurement systems: an Acoustic Concentration and Velocity Profiler (ACVP) (Hurther et al., 2011) and Conductivity Concentration Profilers (CCP) (Lanckriet et al., 2013; Mieras et al., 2017) at two vertical resolutions (1 and 2 mm). This study marks the first use of the 2-mm CCPs. It is also the first time the CCP technology has been used with lightweight acrylic particle flows driven by steady, unidirectional gravity currents. The main objective of this study is to evaluate the performances and limitations of the above mentioned measurement techniques, the ACVP and the CCPs, for (i) measuring time-resolved and average sediment concentration profiles over the entire sediment transport layer and for (ii) tracking the temporal bed level evolution and sheet flow layer thickness. Section 2 presents the experimental setup and protocol, section 3 describes the measurement principles and calibration procedures of the ACVP and CCP technologies, and the results of the comparative analysis are discussed in section 4.

2. Experiment

2.1. Experimental Facility and Flow Conditions

The experiments were carried out at the Laboratory of Geophysical and Industrial Flows (LEGI) in the LEGI/ENSE3 tilting flume (Figure 1). The experimental facility is described extensively in Revil-Baudard et al. (2015) and Revil-Baudard and Chauchat (2013). The flume is L = 10 m long and W = 0.35 m wide, with an adjustable bed slope S_0. A particle pit that is L_p = 3 m long by z_p = 0.11 m deep is mounted at the channel bed 2 m upstream of the channel outlet (Figure 1).

Irregularly shaped polymethyl methacrylate (PMMA) particles (Figure 2) were used with a density of ρ_p = 1,192 kg/m^3. Two particle sizes were used in separate experiments, the coarse S3 and fine S1 particles with median particle diameters, d_p, of 3.0 and 1.0 mm, respectively. The mean settling velocity w_s was 5.5 cm/s for S3 and 2.0 cm/s for S1 (see Table 1). A specific flow condition (i.e., water discharge and bed slope) was set for each particle size to achieve similar Shields numbers. The bed slope was set to 0.0025 for S1 and to 0.0050 for S3, with an average water discharge flow rate, Q_f, of 0.028 and 0.021 m^3/s for S3 and S1, respectively (Table 1).

2.2. Instrumentation Setup

The ACVP was positioned at the downstream end of the particle pit (x = 2.64 m) to collect vertical profiles of velocity and sediment concentration along the vertical flow z direction over a distance of 0.15 m above the initial flat bed level (Figure 1). Two pairs of CCPs were installed to measure vertical concentration profiles along the flow normal z direction. The vertical resolution was 1 mm for the pair of CCP$_{1mm}$ probes, and 2 mm for the pair of CCP$_{2mm}$ probes. Each pair of CCPs was aligned in the streamwise direction, 0.145 m away from the flume walls, and 0.035 m apart from each other in the streamwise direction (Figure 1b). The two CCPs with the same resolution were mounted with a vertical offset, overlapping by a few millimeters to increase the total vertical profiling range. The downstream probes of each CCP pair were positioned

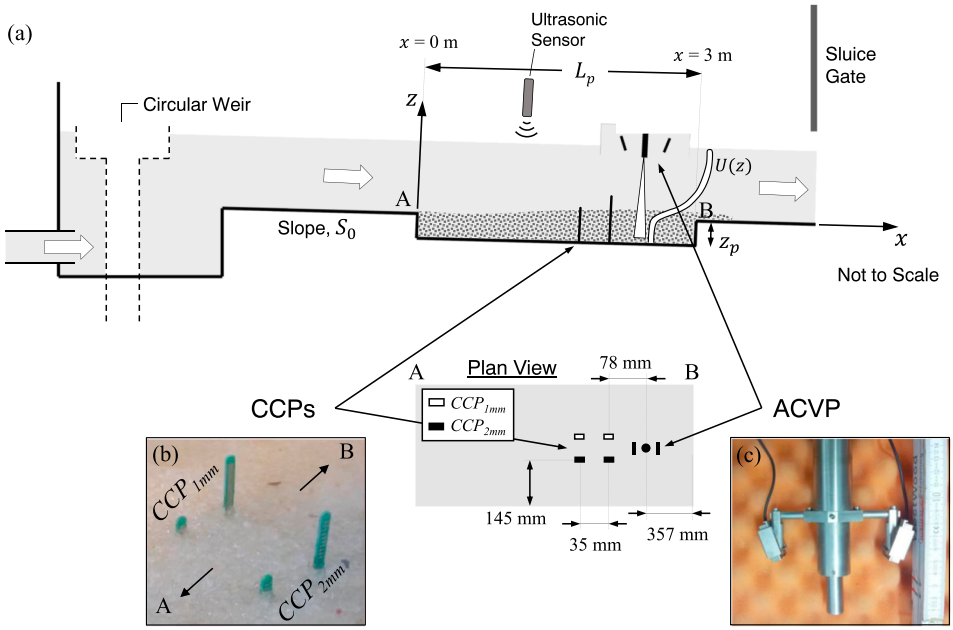

Figure 1. (a) Sketch of the experiment under active flow and location of the instruments. A and B delineate the upstream and downstream edges of the sediment pit, at x = 0 m and x = 3 m, respectively. (b) Picture of the CCP probes deployed before a S3 run. (c) Picture of the ACVP. CCP = Conductivity Concentration Profiler; ACVP = Acoustic Concentration and Velocity Profiler.

0.078 m upstream from the ACVP at x = 2.56 m. The streamwise shift avoided acoustic echoes from the CCP probes in the ACVP signal. An ultrasonic limnimeter was mounted on the trolley to measure the instantaneous water surface. The signal of the ultrasonic limnimeter was simultaneously recorded by the ACVP and the CCP systems allowing time referencing of all data in the postprocessing phase (see section 2.3).

2.3. Experimental Protocol

The experimental protocol described in Revil-Baudard et al. (2015) was applied for each experimental run (Figure 1). Before the start of each run, the particle pit was filled with sediments, manually compacted, and leveled as a flat uniform sediment bed of constant slope. In order to minimize the duration of transient flow until the target discharge was reached, the flume was filled with no particle movement until the still water

Figure 2. PMMA particles used in the S3 (left, d_p= 3 mm) and S1 (right, d_p= 1 mm) experiments. PMMA = polymethyl methacrylate.

Table 1
Flow and Particles Parameters for S1 and S3 Experiments: Bed Slope (S_0), Particle Diameter (d_p), Run Number (N), Fall Velocity (w_s), Particle Density (ρ_p), Friction Velocity (u_*), Water Level (H_f), Flow Rate (Q_f), Mean Bulk Flow Velocity (U), Solid Load Per Unit Width ($q_{s,w}$), Shields Number (θ), Suspension Number ($^{w_s}/_{u_*}$), Mean Dimensionless Flux ($\psi = q_{s,w}/\sqrt{\Delta\rho/\rho_f g d_p^3}$), and Reynolds Number (Re), Where $\Delta\rho$ = 192 kg/m^3 and ρ_f = 1,000 kg/m^3

	S_0	d_p	N	w_s	ρ_p	u_*	H_f	Q_f	U	$q_{s,w}$	θ	$\frac{w_s}{u_*}$	ψ	Re
	(–)	(mm)	(–)	(cm/s)	(kg/m^3)	(cm/s)	(m)	(m^3/s)	(m/s)	(m^2/s)	(–)	(–)	(–)	(–)
S3	0.005	3.0	6	5.5	1,192	4.1	0.14	0.028	0.57	2.7×10^{-4}	1.2	1.3	3.7	8×10^4
S1	0.0025	1.0	3	2.0	1,192	2.1	0.13	0.021	0.46	8.4×10^{-4}	1.7	1	6.3	6×10^4

Note. Note that the hydraulic parameters given here only concern the quasi-steady phase of the flow (see section 4.1).

level was slightly above the aimed normal flow depth. At this stage, the sluice gate at the flume outlet was still closed and a circular weir located at the upstream end of the flume bypassed any additional water discharge, resulting in negligible flow rate over the test section. An initial topographic survey of the particle pit was carried out by towing the ACVP mounted on a trolley, along the flume centerline between positions B and A (see Figure 1). The survey data were used to estimate the initial sediment volume assuming a spanwise-uniform flat bed with a constant packed bed porosity of 45%. The two downstream CCP probe pairs were then manually raised to the desired vertical positions from beneath the flume. The probes were equipped with a cylindrical collar to ensure identical vertical positioning for each repeated run. The vertical position of each pair of CCPs was sufficient to cover the entire thickness of the mobile sediment layer (i.e., from the undisturbed bed to the top of the dilute suspension layer). The ACVP was positioned at x = 2.64 m (Figure 1) before starting the experiment. An experimental run was initiated by rapidly opening the sluice gate at the outlet of the channel, provoking a sudden water level drop that deactivated the circular overflow-weir and transferred the entire flow discharge into the flume. The start time (i.e., t = 0 s) was defined for each run as the instant the water level—recorded by the ultrasonic sensor—dropped to 95% of its original level.

After a period of transient flow lasting about 30 s (Revil-Baudard et al., 2015), the fluid flow and the particle transport layer became fully developed with a normal flow depth of H_f = 0.14 m (0.13 m) and a mean bulk flow velocity of U = 0.57 m/s (0.46 m/s) for S3 (S1). After a duration of about 2 min, the sluice gate was closed to end the run, and the original still water level, for which the circular weir at the upstream end of the flume bypassed the discharge, was recovered. A postexperiment topographic survey was conducted by traversing the ACVP along the flume from B to A (see Figure 1a). The topographic surveys were used to estimate the total volume of transported sediments for each run (using the assumption of spanwise topographic uniformity). After each run, the height of the CCP probes, relative to the bottom of the particle pit, was measured. The experimental protocol was repeated for N = 6 runs for the coarse particles (S3) and N = 3 runs for the fine particles (S1) which provided a sufficient amount of data to minimize the bias errors of the statistical flow quantities (Revil-Baudard et al., 2015). For each run, z = 0 m was defined as the initial bed elevation at t = 0 s.

3. High-Resolution Measurement Systems

3.1. CCP

3.1.1. Concentration Measurements

The CCP measures conductivity of a fluid-particle mixture, σ_m, which is related to volumetric particle concentration via Archie's Law (Archie, 1942; Lanckriet et al., 2013),

$$\frac{1}{F} = \frac{\sigma_m}{\sigma_f} = (1 - \phi)^m, \tag{1}$$

where F is the form factor, σ_f is the conductivity of the fluid, and m is a calibration factor. Each CCP probe has 32 plate electrodes spaced at either 1 or 2 mm vertical increments, resulting in a vertical profile of volumetric particle concentration, $\phi(z)$, spanning either 29 or 58 mm, respectively. All of the CCPs recorded profiles at 8 Hz. An m value was determined for each CCP and experiment using in situ conductivity data and the two-point calibration method outlined by Lanckriet et al. (2013) where ϕ_0 = 0.55 was used as the volumetric concentration of the fully packed bed. The average value of m ($\overline{m}$) across all experiments was 1.3 (1.5) for CCP_{1mm} (CCP_{2mm}). Values for $\overline{m}$ were smaller for the coarse particles (S3) compared to the fine particles

Table 2
CCP Calibration Parameters

	CCP_{1mm}		CCP_{2mm}	
Experiments	$\overline{m}$	σ_{std}	$\overline{m}$	σ_{std}
S3	1.2	0.11	1.5	0.08
S1	1.5	0.02	1.6	0.03

Note. CCP = Conductivity Concentration Profiler.

(S1; Table 2;). Standard deviations, σ_{std}, about $\overline{m}$ were larger for S3 compared to S1 (Table 2), likely due to lower homogeneity of $\phi(z)$ in the packed bed across experiments for the more irregularly shaped grains of S3. The effect of lower homogeneity with S3 is exacerbated for the 1-mm CCPs (i.e., $\sigma_{std,\ S3} = 5.5\sigma_{std,\ S1}$), because the presence of a large void space near a CCP_{1mm} probe influences twice as many measurement bins versus CCP_{2mm} probes.

3.1.2. Bed Interface Detection and Sheet Flow Layer Thickness

The bed interface, $z_b(t)$, was determined by fitting a composite power law and linear curve to the convolution of each instantaneous CCP concentration profile with a boxcar window (width of three measurement bins) to identify the sharp shoulder transition in each sheet flow concentration profile (Lanckriet et al., 2014; Mieras et al., 2017; O'Donoghue & Wright, 2004). The upper boundary of the sheet flow layer, $z_t(t)$, was determined by locating the 8% volumetric concentration contour ($\phi = 0.08$), as is commonly done in sheet flow studies (Ribberink et al., 2008). At concentrations greater than 0.08, the average distance between spherical particles is less than one particle diameter (Bagnold, 1956), and particle-particle interactions become important. The upper boundary of the sheet flow layer was obtained from the same convolved instantaneous CCP concentration profiles used to identify the bed interface. The difference in elevation between the top and bottom of the sheet layer yields the *observed* sheet layer thickness, $\delta_{s,\ sens}(t)$,

$$\delta_{s,sens}(t) = z_t(t) - z_b(t). \tag{2}$$

However, the finite nature of the vertical measurement extent for the CCPs means that observed sheet thicknesses may be overestimated, relative to the true sheet thickness, and a correction formula must be used to convert observed sheet layer thickness to *actual* sheet layer thickness, δ_s,

$$\delta_s = \delta_{s,sens} * \left(\frac{1}{A \times \left(\delta_{s,sens}\right)^2 - B\left(\delta_{s,sens}\right) + C} + 1 \right)^{-1}, \tag{3}$$

where the coefficients A, B, and C for each CCP size are given in Table 3 (Lanckriet et al., 2014). After applying the correction for sheet thickness using equation (3), values of δ_s less than 5 mm (3.6 mm) for CCP_{1mm} (CCP_{2mm}) are not reliable, as they are dominated by profile smoothing, and must be discarded.

The measurement volume, V_{meas}, for CCP_{1mm} is roughly 765 mm^3, based on the volume approximated by an ellipsoid with semiaxes lengths of x = 8.7 mm, y = 8.4 mm (Lanckriet et al., 2013), and z = 2.5 mm. In comparison, the measurement volume for the 2-mm CCP, based on an ellipsoid with semiaxes lengths of x = 15.8 mm, y = 15.6 mm, and z = 1.8 mm (half of the smallest sheet flow thickness that is resolved by the 2-mm CCP), is 1,858 mm^3, 2.4 times larger than for a 1-mm probe. Assuming a linear concentration profile from 0.08 to 0.55 and spherical particles, the measurement volume with a 1-mm CCP would contain 17 (460) particles with diameter of 3.0 mm (1.0 mm). For a 2-mm CCP probe, the number of particles contained within the measurement volume increases to 41 (1,117) for spherical particles with diameter of 3.0 mm (1.0 mm).

3.2. ACVP

3.2.1. Velocity Measurements

The ACVP technology proposed by Hurther et al. (2011) provides time-resolved 1-D vertical profiling of the two components velocity field (as u and w for streamwise and vertical flow velocity components, respectively) and the volumetric sediment concentration. The latter is obtained from the inversion of acoustic intensity profile observations (see following section) which is combined with the simultaneous and colocated velocity measurement to provide horizontal and vertical particle flux profiles at spatiotemporal rates resolving a wide range of the turbulent flow scales. The velocity measurement principle relies on the use of multibistatic pulse-coherent Doppler technology (Hurther & Lemmin, 2001, 2008). The ACVP is composed of one central transmitter with two bistatic receivers in the streamwise plane. Estimates of the quasi-instantaneous Doppler

Table 3
Coefficients for Sheet Flow Thickness Correction Formula, Equation (3), and Minimum Sampling Volumes

	A (m^{-2})	B (m^{-1})	C (–)	V_{meas} (mm^3)
CCP_{1mm}	7.13×10^5	6,024	21.9	765
CCP_{2mm}	2.08×10^5	1,723	3.9	1,858

Note. CCP = Conductivity Concentration Profiler.

frequencies using the pulse-pair algorithm at the two receivers are then converted into the desired (u, w) velocity profile considering the transformation matrix associated with sensor geometry and positioning relative to flow orientation. The unique high-resolution sediment flux measurement ability of the ACVP has recently provided new insights into a variety of wave- (Chassagneux & Hurther, 2014; Hurther & Thorne, 2011; van der Zanden et al., 2016) and current-driven (Naqshband, Ribberink, Hurther, Barraud, et al., 2014; Naqshband, Ribberink, Hurther & Hulscher, et al., 2014; Revil-Baudard et al., 2015, 2016) boundary layer sediment transport processes.

3.2.2. Concentration Measurements

The ACVP was set to operate at an acoustic frequency of 1 MHz, with a pulse duration of 2 μs, allowing a vertical resolution of 1.5 mm and temporal resolutions of 78 and 4.9 Hz for the velocity and concentration measurements, respectively. The volumes sampled by the ACVP increase along the profile due to spherical spreading and reach approximately 250 mm^3 at z = 0.1 m away from the emitter (corresponding to an equivalent circular patch of 15-mm diameter on the horizontal direction with a vertical resolution of 1.5 mm). Note that the lower temporal resolution for the concentration measurements comes from the necessity of incoherent scattering conditions implying that the backscattered signal has random phase statistics uniformly distributed over 2π. In our highly turbulent flow conditions, this requirement is typically fulfilled at a maximum temporal rate of about 5 Hz which induces a statistical bias error of less than 20% for the time-resolved concentration data. Because the pressure amplitude realizations are statistically Rayleigh distributed, the bias error of the concentration moments decreases with population size to the power of -0.5 (Bricault, 2006; Thorne & Hurther, 2014).

Under incoherent scattering and negligible multiple scattering conditions, the output intensity signal of the ACVP is written as (Hurther et al., 2011):

$$I = A_j A_s \rho_p \phi \exp\left(-4\int_0^r \zeta_s \rho_p \phi \mathrm{d}r\right), \tag{4}$$

where

$$A_j = R_0^2 \frac{\tau c}{4} \exp(-4\alpha_w r), \tag{5}$$

$$A_s = \frac{3}{4\rho_p} \frac{\{a^2 f^2(\theta = \pi, ka)\}}{\{a^3\}}, \tag{6}$$

$$\zeta_s = \frac{3}{4\rho_p} \frac{\{a^2 \chi(ka)\}}{\{a^3\}}. \tag{7}$$

The term A_j includes the system-dependent parameters and the water absorption term along the profile; R_0 is a system constant containing the transducer sensitivity and transfer function of the hardware unit (Bricault, 2006; Hurther et al., 2011); τ is the pulse duration; r the range from the transducer; c is the speed of sound in water; α_w is the water absorption coefficient (Thorne & Hurther, 2014). The term A_s is the particle backscattering constant (Thorne & Hanes, 2002) and ζ_s is the attenuation coefficient. The term ka is the product of the wave number, k, and particle radius, a. The functions f and χ are, respectively, the intrinsic form function in the backscattered direction, describing the backscattering characteristics of the suspended particles, and the total scattering cross section, describing the scattering attenuation characteristics of the suspension along the acoustic path at a distance r from the emitter.

For spherical PMMA particles of density ρ_p = 1,192 kg/m^3, compressional and shear velocities c_p = 2,690 m/s and c_s = 1,340 m/s, and assuming a water density and sound velocity of 1,000 kg/m^3 and 1,480 m/s, respectively, f and χ were computed following Thorne and Campbell (1992). The scattering angle θ is set to π corresponding to the backscattered sound. Curly brackets {} denote the average over the particle size distribution $n(a)$ in suspension, such that the volumetric concentration can be written as

$$\phi = N_p \frac{4}{3}\pi \int_0^\infty a^3 n(a) \mathrm{d}a, \tag{8}$$

where N_p is the numerical particle density (number/m^3) of mean radius $a_s = \{a\} = \int_0^\infty a n(a) \mathrm{d}a$. When A_j, f, χ, a_s, and $n(a)$ are known a priori, it is possible to evaluate the volumetric concentration profile, $\phi(z)$, by

inverting equation (4) using a direct implicit iterative approach, the performances and limitations of which are addressed in Hurther et al. (2011) and Bricault (2006). Note that in both S1 and S3 cases, the water column contains micro air bubbles used as flow tracers with negligible inertial lag relative to the elementary fluid parcels. This guaranties the continuous measurement of flow velocity over the entire water column. However, the intensity scattered by these micro air bubbles remains negligibly low compared the acoustic intensity scattered by the suspended solid particles, especially in the used megahertz frequency range. The air bubble intensity is first determined from clear water experiments in identical hydraulic flow conditions and is subtracted (as a background intensity level) from the total received intensity measured in the sheet flow experiments (Bricault, 2006). The resulting air bubble intensity typically corresponds to a negligible particle concentration lying in the 10-mg/L range. Measurements in the bedload layer are therefore insensitive to this intensity correction.

3.2.3. Bed Interface Detection

The Acoustic Bed Interface Tracking (ABIT) method proposed by Hurther and Thorne (2011) is implemented into the ACVP technology. It enables the separation of the total acoustic intensity within the same measurement volume (often referred to as a bin) into the intensities scattered by the moving and the nonmoving particles. The nonmoving sediments are associated with the particles constituting the undisturbed bed. The corresponding acoustic intensity is called the bed intensity. The separation of the total intensities relies on the use of the frequency demodulated Doppler signal for the estimation of the acoustic intensity, the Doppler signal being constant when generated by a nonmoving target. As a result, the localization of the peak intensity in the vertical bed intensity profiles is associated with the position of the undisturbed bed, noted z_b. The ABIT method was used here for the time-resolved detection of the undisturbed bed level below which the instantaneous velocity and concentration are forced to zero and to ϕ_0, respectively. Due to the strong acoustic signal loss inside the dense sheet flow layer, the raw intensity profiles were corrected for particle scattering attenuation before the ABIT method is applied.

3.3. Validation of Acoustic Transport Rate Measurements

Before looking into the detailed comparison of the conductivity and acoustic measurements (section 4), the acoustic sediment transport measurements are validated. The validation relies on a volume balance approach comparing the total volume of transported sediments estimated from the topographic surveys to the transported volume estimated from the sediment flux profiles provided by the ACVP. In this section, the topographic survey method is first described. Because the S1 particles were measured acoustically for the first time, the determination of the acoustic inversion parameter is explained (section 3.3.2). Then, comparison of the topographically and acoustically estimated sediment volumes for all runs is discussed in terms of transport rate measurement accuracy (section 3.3.3).

3.3.1. Topographic Estimation of Transported Particle Volume

For each run, topographic surveys were used to estimate the total transported particle volume following the towing procedure described in section 2.3. The ACVP recorded acoustic intensity and velocity profiles while it was towed over the particle pit. A reference bed level was determined before and after each experiment above the rigid bed ends adjacent to the edges of the particle pit (labeled as points A and B in Figure 1a). This reference bed level is common to all initial and final topographic surveys. The bed level based on topography bed scans, $z_b(x)^{\mathrm{Topo}}$, was defined by the peak value in the acoustic profiles (Figures 3b and 3d). As the ACVP was towed relative to the bed, the bed velocity measured at the elevation of peak intensity corresponds to the trolley speed. The instantaneous velocities of the towed ACVP trolley relative to the fixed tilted flume (Figures 3a and 3c) were integrated over time to determine the instantaneous horizontal position of the trolley over the particle pit. Finally, the total transported particle volume, V_{Topo}, was determined by subtracting the topographic elevations before and after each run and integrating over the length of the particle pit located upstream from the ACVP position during each run x_{ACVP} (see Figure 1),

$$V_{\mathrm{Topo}} = W\phi_0 \int_0^{x_{\mathrm{ACVP}}} \left[\left(z_b(x)^{\mathrm{Topo}} \right)_{\mathrm{After}} - \left(z_b(x)^{\mathrm{Topo}} \right)_{\mathrm{Before}} \right] \mathrm{d}x \tag{9}$$

It is assumed in equation (9) that the packed bed concentration, ϕ_0, is spatially homogeneous in the postrun bed and that the bed along the flume centerline is representative of the spanwise averaged bed elevation. The last assumption is strongly supported by the visual inspection of two-dimensional bed topography over the entire length of the sediment pit.

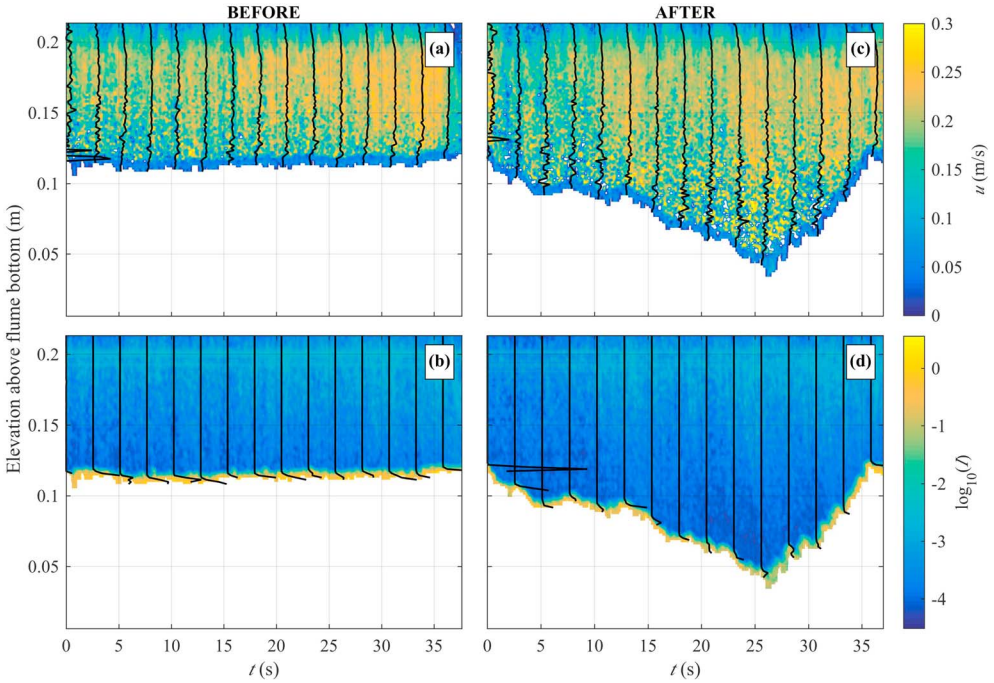

Figure 3. Example time-space color plots of (a, c) streamwise velocity and (b, d) logarithm base 10 of the acoustic intensity measurements during a topographic survey conducted (a, b) before and (c, d) after an experimental run. The black lines represent instantaneous profiles at intervals of approximately 3 s, where the time range on the *x* axis is the duration of time over which the trolley traversed the 3-m-long particle pit.

3.3.2. Acoustic Inversion Parameters

For the experiments with the coarse S3 particles, the inversion parameters $A_j A_s$ that were previously determined in Revil-Baudard and Chauchat (2013) and Revil-Baudard et al. (2015, 2016) are used to perform the implicit acoustic inversion as described in Thorne and Hurther (2014), yielding volumetric concentration profiles. Since no direct calibration of the fine S1 particles is available, the scattering constant, A_s, equation (6), as well as the attenuation coefficient ζ_s, equation (7), must be evaluated using the theoretical backscattering properties of PMMA particles. No exact backscattering model exists to describe the scattering properties of irregularly shaped PMMA particles, so the assumption is made here that the employed particles can be approximated to perfectly spherical particles. The ensemble average of f and χ were taken over the total size distribution, following $\{f\} = \left(\frac{\{a\}\{a^2 f^2\}}{\{a^3\}}\right)^{0.5}$ and $\{\chi\} = \frac{\{a\}\{a^2\chi\}}{\{a^3\}}$. In order to invert the acoustic signal for the fine particles, the empirically determined constant $A_j A_s$ is thus corrected from the ratio $\frac{\{f_{S1}\}}{\{f_{S3}\}}$

$$\left(A_j A_s\right)_{S1} = \left(A_j A_s\right)_{S3} \frac{\{f_{S1}\}}{\{f_{S3}\}}, \tag{10}$$

and the attenuation coefficient, ζ_s, is calculated from equation (7). The inversion of ACVP backscattered intensities to volumetric concentration, ϕ, then follows the same implicit scheme of Thorne and Hurther (2014) as for the S3 particles.

3.3.3. Comparison Between Topographic and Acoustic Estimations

The instantaneous transport rate $q_s(t)$, and temporal evolution of the transported volume of particles at the location of the ACVP, $V_{\mathrm{ACVP}}(t)$, were computed from the ACVP for S3 and S1 by cumulatively integrating the vertically integrated streamwise flux over time (Figures 4a and 4b),

$$q_s(t) = W \int_{z_b(t)}^{H_f} u(z,t)\phi(z,t)\mathrm{d}z \tag{11}$$

$$V_{\mathrm{ACVP}}(t) = W \int_0^t \int_{z_b(t^*)}^{H_f} u(z,t^*)\phi(z,t^*)\mathrm{d}z\mathrm{d}t^* \tag{12}$$

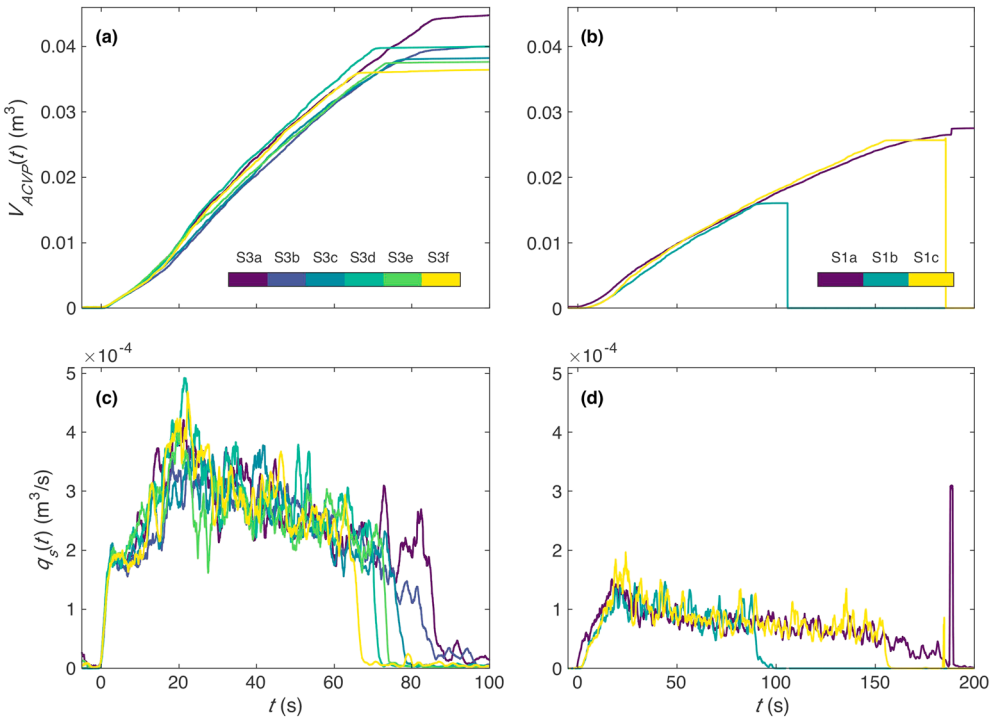

Figure 4. Time evolution of (a, b) the cumulative transported particle volume derived from ACVP measurements, $V_{ACVP}(t)$ (equation (12)), and (c, d) particle transport rate (filtered at 1 Hz) derived from ACVP measurements, $q_s(t)$, for all N runs of the S3 (a, c) and S1 (b, d) conditions (equation (11)). ACVP = Acoustic Concentration and Velocity Profiler.

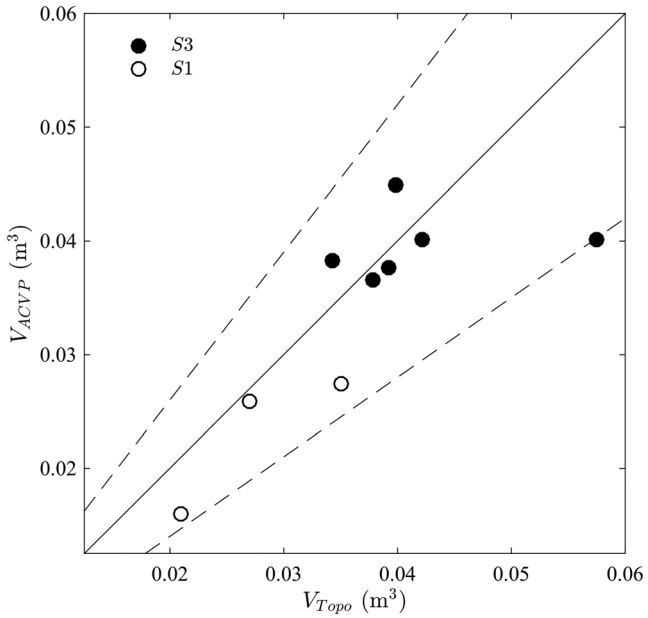

Figure 5. Comparison between the total transported particle volume estimates for all runs during the S3 and S1 conditions, from the topographic surveys (V_{Topo}; equation (9)) and from ACVP measurements (V_{ACVP}; equation (12)). The solid line represents a 1:1 match, and the dashed lines correspond to an uncertainty of ±30%. ACVP = Acoustic Concentration and Velocity Profiler.

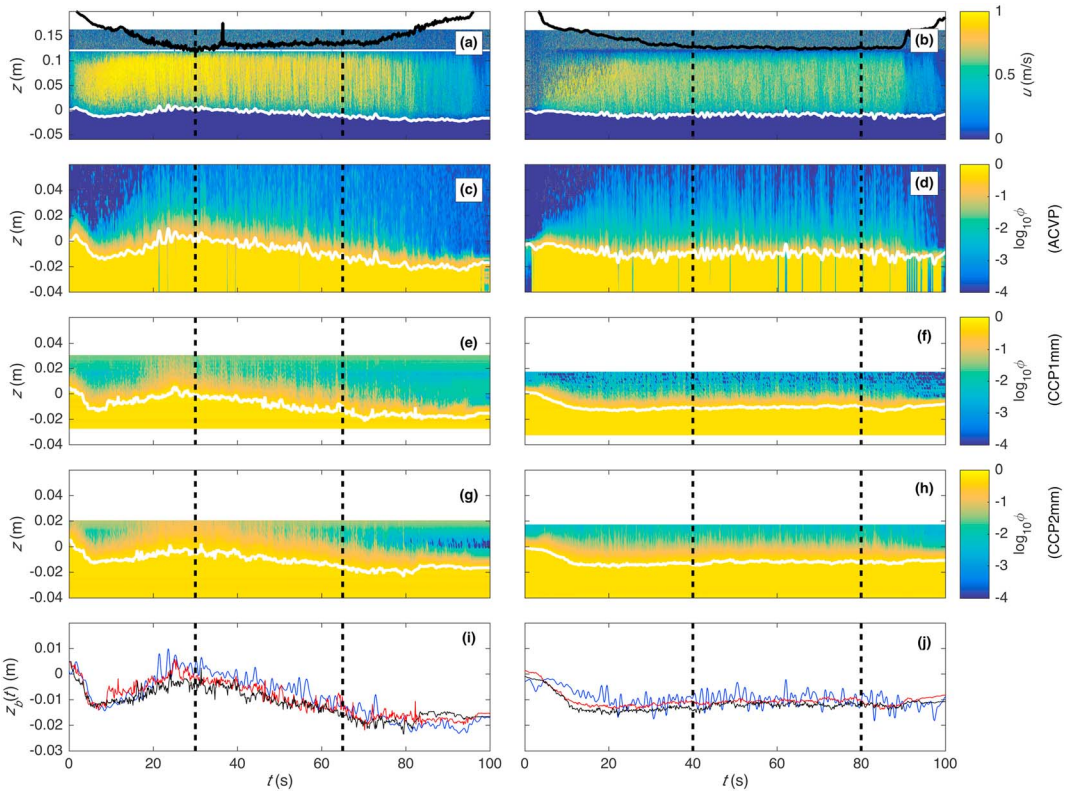

Figure 6. Time-space plots of (a, b) streamwise ACVP velocity, (c, d) ACVP-derived concentration, (e, f) CCP_{1mm}-derived concentration, (g, h) CCP_{2mm}-derived concentration; and (i, j) bed interfaces derived from ACVP (blue line), CCP_{1mm} (red line), and CCP_{2mm} (black line) bed interfaces for trials S3b (left column) and S1b (right column) experiments. The black lines in (a, b) represent the instantaneous free surface. The white lines are the bed interfaces estimated from ACVP (see section 3.2) and CCP (see section 3.1) data. The vertical dashed black lines denote the quasi-steady time interval over which the data are time averaged. ACVP = Acoustic Concentration and Velocity Profiler; CCP = Conductivity Concentration Profiler.

First, it can be observed that the runs were reasonably repeatable for both S1 and S3 experiments. The duration of each run, T, was slightly different, where the end of a run (i.e., when the sluice gate was closed) is denoted by the sudden flattening (i.e., plateau) of $V_{ACVP}(t)$, indicating that no additional volume of particles was being transported (Figures 4a and 4b). The instantaneous transport rate, $q_s(t)$, is presented Figures 4c and 4d. The transport rate reached a maximum around t= 20 s, then remained roughly constant after $t\approx$ 30 s ($t\approx$ 60 s) for the S3 (S1) condition before sharply decreasing to 0 at the end of each run ($t = T$), as the sluice gate was lowered and the flow discharge dropped to 0. The accuracy of the ACVP-derived particle fluxes was evaluated by comparing the total volume of particles transported for each run estimated from the ACVP measurements, with the total transported particle volume estimated from topographic surveys (V_{Topo}; equation (9) and Figure 5). It can be seen that all acoustically estimated volumes are contained within an uncertainty range of ±30% (Figure 5, dashed lines) which strongly supports the transport rate measurement ability of the ACVP technology.

4. Intercomparison of CCP and ACVP Systems

This section details the intercomparison of ACVP and CCP measurements. Time-resolved concentration profiles are first analyzed as a function of free-surface elevation and the velocity profiles obtained with the ACVP. The time-resolved detection of the bed interfaces are compared and analyzed (section 4.2). The intercomparison of averaged velocity, concentration, and sediment flux profiles across the sheet flow and suspension layers are investigated in section 4.3.1. The ensemble-averaged time-varying and time-averaged sheet flow layer thickness estimates are then compared in section 4.3.2.

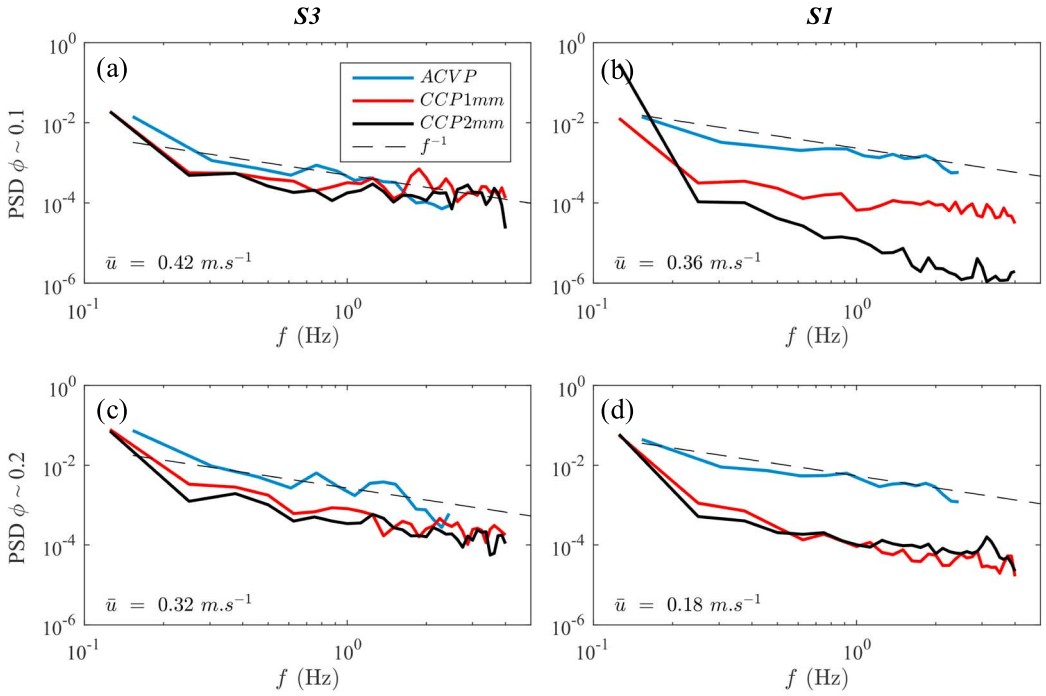

Figure 7. Concentration spectra observed for the ACVP (blue line), CCP_{1mm} (red line), and CCP_{2mm} (black line) during two representative runs of the S3 (a, c) and S1 (b, d) experiments at two elevations corresponding to averaged concentrations of $\overline{\phi} = 0.1$ (a, b) and $\overline{\phi} = 0.2$ (c, d). The mean velocity $\overline{u}$ over the averaging period is indicated in the bottom left corner of each panel. ACVP = Acoustic Concentration and Velocity Profiler; CCP = Conductivity Concentration Profiler.

4.1. Time-Resolved Velocity and Concentration Measurements

Figure 6 presents time-space color plots of the time-resolved velocity profiles (ACVP) and concentration profiles (ACVP and CCPs) together with the time series of the undisturbed bed level (ACVP and CCPs; see sections 3.2 and 3.1 for the methodologies), for a representative run of the S3 and S1 experiments (named S3b and S1b in Figure 6, corresponding to the S3b and S1b experiments in Figure 4). Only one run per condition is shown here for brevity; the same figure is available for each run as supporting information.

Consistent with Figure 4, the initial response was characterized by a transient phase lasting about 40 s (60 s) for S3 (S1), with rapidly increasing velocities, reaching 1.1 m/s (0.95 m/s) at t= 20 s (10 s) for S3 (S1), before decreasing with time until t= 30 s (40 s) for the S3 (S1) condition (Figures 6a and 6b). Concurrently, the color plots of concentration in Figure 6 reveal that during the first 20 s of the experiments, the suspension steadily grew in time, reaching higher elevations. After the transient phase, the flow reached a quasi-steady bed erosion phase, where the measured velocities stabilized over a period of time between t= 30–65 s for S3 and t= 40–80 s for S1 (Figure 6). This effect can also be visually inferred from the bed level evolution being horizontal for both the ACVP and CCPs over the same time windows (Figures 6i and 6j), as well as from the steadiness of the free-surface elevation (black solid lines in the time intervals between the two vertical dashed lines in Figures 6a and 6b). At the end of each experiment, the sluice gate was closed, which led to a rapid decrease of the flow rate as the water level rose back to the initial still water level. Note that this instant in time differed for each run (see Figure 4), since the sluice gate was lowered manually at the end of each run at different instants.

Qualitatively, both the CCP and ACVP concentrations exhibit highly intermittent concentration variations in the near bed region. These dynamics were shown previously to be driven by highly intermittent large-scale turbulent flow structures identified as ejection and sweep events in Revil-Baudard et al. (2015). However, no direct comparison of the instantaneous events based on observations is possible due to the following: (i) the horizontal (0.078 m) and lateral (0.03 m) offsets in the ACVP and CCP positioning, and (ii) the fact that the CCP data were merged from a pair of sensors that were offset vertically and horizontally by 0.035 m (Figure 1b). At some instants, the ACVP concentration time series was marked with suspiciously low concentrations in the bed (Figures 6c and 6d). At these few events per run, the suspended layer was so thick that the acoustic

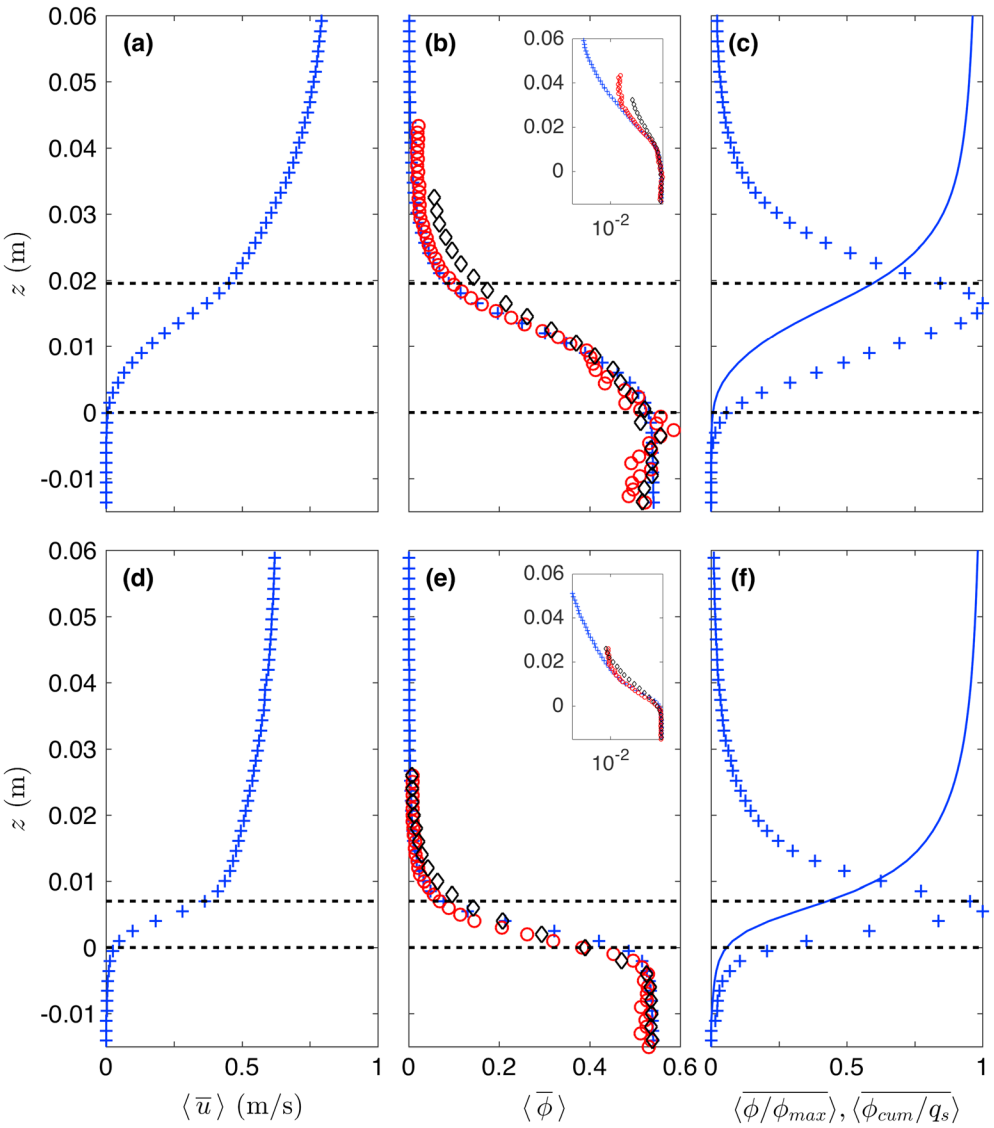

Figure 8. Ensemble-time-averaged (a, d) velocity profiles, (b, e) concentration profiles, and (c, f) particle volume flux profiles for (a–c) S3 and (d–f) S1. In panels (b, e), the concentration was measured by the ACVP (plus), CCP_{1mm} (circles), and CCP_{2mm} (diamonds). The same concentration data are plotted in semilogarithmic scale (insets) to highlight the suspension layer (i.e., $\langle\overline{\phi}\rangle < 0.08$). The blue lines in panels (c, f) are normalized, cumulative sum of the volume flux. In each panel, the dashed black lines show the mean upper sheet flow layer interface (where $\langle\overline{\phi}\rangle = 0.08$) and the mean bed position. ACVP = Acoustic Concentration and Velocity Profiler; CCP = Conductivity Concentration Profiler.

signal could not reach the true packed bed concentration value of 55% at the position of the undisturbed bed detected correctly with the ABIT method. This undesired behavior is attributed to the insufficiently compensated acoustic attenuation due to local multiple scattering effects modeled with a simplistic first order approximation in equation (4). However, such events were rare and can be detected easily in the bed level time series provided by the ABIT method.

In order to compare the measured time variability relative to each other, the concentration spectra are shown in Figure 7 at two elevations inside the bedload layer for the S3 (Figures 7a and 7c) and S1 (Figures 7b and 7d) conditions corresponding to time-averaged concentrations $\overline{\phi} = 0.1$ (z= 0.018 m for S3 and z= 0.007 m for S1) and $\overline{\phi} = 0.2$ (z= 0.015 m for S3 and z= 0.004 m for S1), respectively. The spectra were computed using Welch's method with 50% overlapping Hanning windows of 512 (64) samples each for the ACVP (CCPs) over a duration of 35 s (40 s) for the S3 (S1) experiment. The spectral range of the acoustic measurements (ACVP) lies in the turbulence production range between 0.1 and 2.45 Hz considering the present fully turbulent flow

Table 4
Average (Mean) and Root-Mean-Square Differences (RMS) of Bed Level Positions Between (a) ACVP and CCP_{1mm}, (b) ACVP and CCP_{2mm}, and (c) CCP_{1mm} and CCP_{2mm}, Normalized by the Particle Diameter During the Transient Phase ($t < 30$ s for S3 and $t < 40$ s for S1) of the Flow and the Quasi-Steady Phase of the Flow for S3 and S1 Experiments (t= 30–65 s for S3 and t= 40–80 s for S1)

	Transient phase				Quasi-steady phase			
	S3		S1		S3		S1	
	Mean	RMS	Mean	RMS	Mean	RMS	Mean	RMS
ACVP versus CCP_{1mm}	0.2	1.5	1.7	3.4	0.9	1.2	1.0	2.6
ACVP versus CCP_{2mm}	0.7	1.8	3.5	4.6	1.4	1.7	2.5	3.7
CCP_{1mm} versus CCP_{2mm}	0.8	1.1	1.8	1.9	0.5	0.8	1.5	1.6

Note. CCP = Conductivity Concentration Profiler; ACVP = Acoustic Concentration and Velocity Profiler.

regime. The spectral range covered by the conductivity measurement (CCP) also lies in the turbulence production range between 0.1 and 4 Hz. The spectra agree in terms of magnitude and shape for the two points in the S3 experiments. For the S1 experiment (Figures 7b and 7d), significant differences are seen with higher values for the acoustic measurements. Although the spectra display a similar behavior for both the S3 and S1 experiments (except for CCP_{2mm} in Figure 7b, where the observed deviation is most likely due to the larger spacing between the electrodes coupled with the low content of particles in the measurement volume, particularly in the more dilute part of the flow—see section 4.3.1 and Figure 8), it appears that the conductivity-based spectra are consistently lower. This could (at least partly) be a consequence of the larger finite extent of the measurement volumes of the CCP systems compared to the ACVP (see sections 3.1 and 3.2). A larger measurement volume is expected to act as a spatial low-pass filter, thus lowering the energy observed on the CCP spectra at higher frequencies.

In the turbulence production range, the acoustic spectra have a slope close to the value of f^{-1} roll off. It is difficult to quantitatively interpret the spectra shape given the relatively sparse data on near bed particle concentration spectra in the literature. However, it is interesting to note that this f^{-1} dependence has also been reported as an empirical result in the recent work of Wilson and Hay (2016). As in the present study, Wilson and Hay (2016) made measurements using a bistatic high-resolution coherent Doppler velocity profiler, under steady flow conditions, but not in the sheet-flow regime (Shields parameter ~ 0.2). The f^{-1} spectra shape seems to be applicable to both flow regimes.

4.2. Time-Resolved Detection of the Bed Interface

Table 4 presents the average and root-mean-square differences of bed level positions observed by the three systems. The CCP-derived bed levels from both CCP_{1mm} and CCP_{2mm} (Figures 6i and 6j) differ by only one to two particle diameters (d_p= 3.0 mm), on average for the S3 experiments, during the transient phase of the experiment (t= 0–30 s, RMS = 1.1 d_p; see Table 4). The agreement is similar for the S1 experiments, during which the interfaces differed by only two to three particle diameters (d_p= 1.0 mm), on average, during the transient phase of the experiment (t= 0–40 s, RMS = 1.9 d_p; see Table 4). Similar trends are observed during the quasi-steady phase.

The overall temporal evolution of the ACVP and CCP measured bed levels was similar during the entire run duration for all nine experiments (see Table 4 and supporting information). During the quasi-steady phase of the flow (between the two vertical dashed lines in Figure 6), the agreement between ACVP-based and CCP-based bed interfaces is good for both S3 (S1) with differences of one to two (three to five) particle diameters, on average (Table 4). During the same period, the average erosion rate over all runs (i.e., the drop of the bed interface with time) was faster for the coarse particles (~ 0.5 mm/s) than for the fine particles (~ 0.2 mm/s; Figures 6i and 6j).

4.3. Average Flow Quantities

4.3.1. Velocity, Concentration and Sediment Volume Flux Profiles

The velocity, concentration, and particle volume flux profiles were time averaged, denoted by $\bar{(\ )}$, over a portion of the quasi-steady phase of each run. During this time the flow is steady and uniform with a

Table 5
Root-Mean-Square Differences of the Observed Concentrations Between the Different Instruments for Different Ranges (Determined Based on the CCPs' working ranges: $\langle\overline{\phi}\rangle > 0.02$ for CCP_{1mm} and $\langle\overline{\phi}\rangle > 0.2$ for CCP_{2mm}) of the Ensemble-Time-Averaged Concentration Profiles

	ACVP versus CCP_{1mm}		ACVP versus CCP_{2mm}	
RMS (–)	S3	S1	S3	S1
Entire $\langle\overline{\phi}\rangle$ profile	0.032	0.032	0.030	0.026
$0.02 < \langle\overline{\phi}\rangle < 0.35$	0.018	0.014	-	-
$0.20 < \langle\overline{\phi}\rangle < 0.35$	-	-	0.018	0.056
$\langle\overline{\phi}\rangle > 0.35$	0.049	0.063	0.027	0.051

Note. CCP = Conductivity Concentration Profiler; ACVP = Acoustic Concentration and Velocity Profiler.

quasi-steady erosion rate (Revil-Baudard et al., 2015). A time length of around 66 s was also shown to be sufficiently long to provide a statistical bias error in the range of 1% for the first-order moments of velocity and concentration profiles (Revil-Baudard et al., 2015). Moreover, this time length was sufficiently long to cover the return time of the largest turbulent flow structures scaling with the flow depth.

The averaging interval was from $t = 30$ s to $t = 65$ s for the S3 experiments and from 40 to 80 s for S1, as indicated by the vertical dashed black lines in Figure 6. These time intervals are longer than the 66 s taken in Revil-Baudard et al. (2015, 2016) to ensure well-converged temporal means. They are represented by the time in between the two vertical dashed black lines in Figure 6. Ensemble-averaging, denoted as $\langle\rangle$, was further carried out over the number of repeated runs (three and six runs for S1 and S3, respectively) to further decrease the statistical bias error in the temporal average.

The ensemble time-averaged velocity profiles in Figures 8a and 8d reveal the existence of an inflection point (so-called *S-shape*) typical under sheet flow conditions (Revil-Baudard et al., 2015; Revil-Baudard & Chauchat, 2013). The inflection point elevations also correspond well with the 8% volumetric concentration elevation (Figures 8b and 8e), which separates the sheet flow layer $\langle\overline{\phi}\rangle > 0.08$ from the upper dilute suspension layer $\langle\overline{\phi}\rangle < 0.08$. As demonstrated in Revil-Baudard et al. (2016), the momentum diffusion processes strongly differ in the two layers; particle-particle collisions and frictional interactions dominate in the sheet flow layer, whereas turbulent mixing dominates in the suspension layer. The shapes of the concentration profiles (Figures 8b and 8e) are also similar to previously observed profiles for sheet flow conditions (O'Donoghue & Wright, 2004). In the sheet flow layer, the concentration decreases almost linearly with z, whereas in the

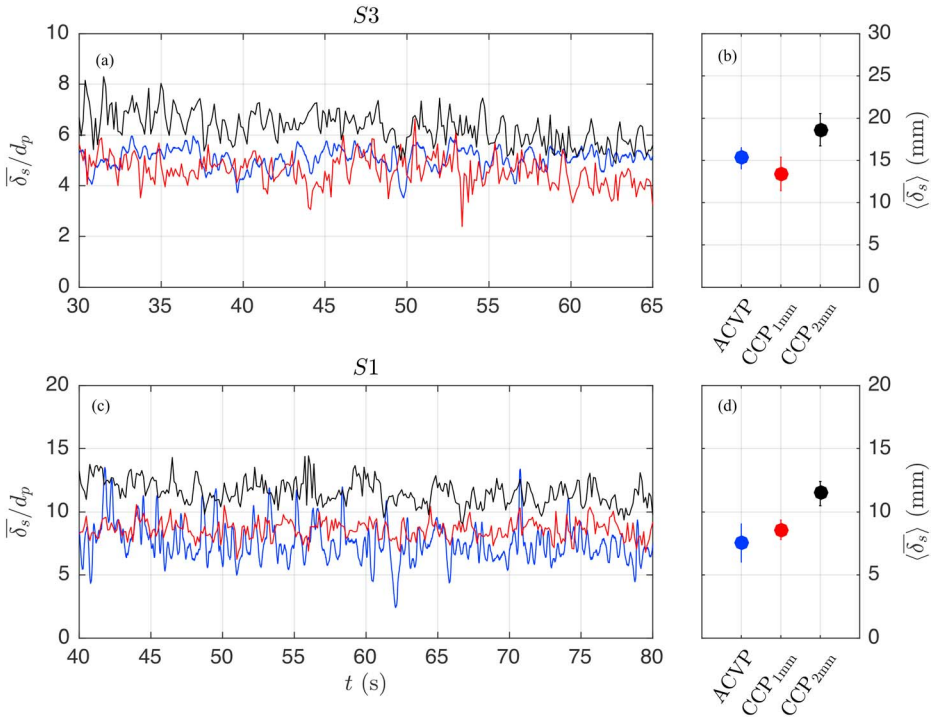

Figure 9. (a, c) Time series of ensemble-averaged sheet flow thickness, $\langle\delta_s(t)\rangle$, normalized by particle diameter, and (b, d) time averages of the ensemble-averaged sheet flow thickness, $\langle\overline{\delta_s}\rangle$, for the ACVP (blue), CCP_{1mm} (red), and CCP_{2mm} (black), with error bars of ±1 standard deviation. The top row (a, b) corresponds to the S3 conditions, while the bottom row (c, d) corresponds to the S1 condition. ACVP = Acoustic Concentration and Velocity Profiler; CCP = Conductivity Concentration Profiler.

Table 6
Ensemble-Time-Averaged Sheet Flow Layer Thickness $\langle\overline{\delta_s}\rangle$ Comparison Between Instruments, Shown With ±1 Standard Deviation

	ACVP	CCP_{1mm}	CCP_{2mm}
S3	15.3 ± 1.3 mm	13.4 ± 2.0 mm	18.7 ± 1.9 mm
S1	7.5 ± 1.5 mm	8.6 ± 0.8 mm	11.5 ± 1.0 mm

upper dilute region, an exponential decay typical of the suspension layer is observed (also called Rouse profile). Figures 8b and 8e present a close-up of the ensemble-time-averaged concentration profiles, with the same data also shown in figure insets with semilogarithmic axes. For the sake of comparison, the RMS of the relative average concentration differences along the profile between the ACVP and CCPs was computed. Good agreement was observed over the entire profile (see Table 5), particularly in the range $0.02 < \langle\overline{\phi}\rangle < 0.35$ for CCP_{1mm} (S3: *RMS* = 0.018; S1: *RMS* = 0.014). In the dense region ($\langle\overline{\phi}\rangle > 0.35$), the ACVP measures slightly larger mean concentration values than the CCPs, especially for the S1 condition (*RMS* = 0.063 for CCP_{1mm} and *RMS* = 0.051 for CCP_{2mm}), while in the dilute region, the CCPs return higher concentration values (Table 5). The overprediction of concentration in the dilute region by CCP_{2mm} appears closer to the bed ($\langle\overline{\phi}\rangle \lesssim 0.2$) compared to CCP_{1mm} ($\langle\overline{\phi}\rangle \lesssim 0.02$) and is probably related to the larger electrode spacing on the probe.

In Figure 8, the nonzero values of the measured quantities below $z = 0$ are due to the definition of origin of the z axis as the ensemble time-averaged bed level position rather than the instantaneous bed position having a high temporal variability. This variability (induced by the bed intermittency) was found to be associated with the dynamics of large-scale turbulent flow structures known as ejection and sweep-type events (Revil-Baudard et al., 2015, 2016).

Figures 8c and 8f show the time-averaged particle volume flux (blue +) and cumulative sum of time-averaged volume flux profiles (blue line), which were directly estimated from the simultaneous and colocated velocity and concentration measurements provided by the ACVP. The peak of particle volume flux is located close to the transition between the sheet flow and the suspension layer $\langle\overline{\phi}\rangle \approx 0.08$, which is consistent with previous studies (Revil-Baudard et al., 2015). It reveals that there is a fairly equal partition between the sheet flow and suspended load contributions to the total net sediment transport.

4.3.2. Sheet Flow Layer Thickness

The experimental data also enable direct comparison of sheet flow thickness estimates measured with the ACVP and CCPs (see section 3.1). Figures 9a and 9c present the time-varying, ensemble-averaged sheet flow thicknesses, $\langle\delta_s(t)\rangle$, obtained for both flow conditions S3 and S1 using the ACVP, CCP_{1mm} and CCP_{2mm} probes. Local differences between each pair of instruments can be seen reaching one (ACVP vs. CCP_{1mm}) to four (ACVP vs. CCP_{2mm}) particle diameters for the S3 experiments (Figures 9a) and three (ACVP vs. CCP_{1mm}) to seven (ACVP vs. CCP_{2mm}) particle diameters for S1 (Figure 9c). Systematic higher sheet flow thicknesses were obtained with the CCP_{2mm} compared with the other instruments as a result of the lower vertical spatial resolution.

Ensemble time-averaged sheet layer thicknesses, $\langle\overline{\delta_s}\rangle$ (Figures 9b and 9d), using both measurement systems (ACVP and CCPs) are in good agreement, with a difference of less than one and two particle diameters for the S3 (Figure 9b) and S1 (Figure 9d) experiments, respectively (Table 6). Systematic larger differences are observed with the CCP_{2mm} with relative values of about four and seven particle diameters for the S3 and S1 conditions, respectively.

5. Conclusions

A detailed comparative analysis of acoustic and conductivity-based measurements was carried out in shear-driven sheet flows with two sizes of lightweight acrylic particles with diameters of 1.0 (S1) and 3.0 mm (S3). The measurement performances and limitations of the systems were evaluated for vertical profiling across the sheet flow and suspension layers of sediment concentration, instantaneous bed level, sheet flow layer thickness, and the sediment transport rate provided by the ACVP system.

The ACVP provides reliable nonintrusive concentration estimates across the entire dilute suspension layer with shapes of the mean profiles following the expected Rouse profile (Revil-Baudard et al., 2015, 2016). This confirms the expected validity and applicability of acoustic scattering-based technologies in dilute sediment suspension flows. Inside the sheet flow layer, good agreements with the CCP concentration measurements are found for $\phi \lesssim 0.35$ which covers 75% and 60% of the range of sheet flow layer thicknesses, for the S3 and S1 conditions, respectively. In the lower sheet flow layer associated with the sediment pick-up layer,

systematic overestimation of the acoustic concentration measurements compared to the CCP concentration measurements were observed. However, when normalized by the local mean concentrations (given by the CCP measurements as reference values), these relative differences are less than 10% in the densest part of the sheet flow layer.

As expected from the conductivity-based measurement principle, the CCP technology provides accurate concentration profiles over the entire dense sheet flow layer associated with $\phi \gtrsim 0.08$. More unexpected is the ability to return accurate concentration estimates in the dilute suspension layer down to concentrations of the order of 1% for the CCP_{1mm} and 10% for CCP_{2mm}, respectively. This demonstrates that with an appropriate vertical resolution (i.e., smaller than the sheet flow layer thickness), the CCP technology provides reliable instantaneous profile data outside its conventional range of application previously thought to be restricted to $\phi >$ 5–8% for CCP_{1mm}.

The observed differences between the two CCPs in terms of lower concentration limit that can be reliably resolved is a consequence of the different measurement volume sizes. In order to reach a representative measurement of the concentration, the latter must be large enough to contain a sufficient number of particles and small enough to minimize spatial smoothing effects (Lanckriet et al., 2014) in the vertical direction. The larger vertical extent of the measurement volume of CCP_{2mm} leads to increased vertical smoothing of the concentration profiles (Lanckriet & Puleo, 2013), hence the observed higher volumetric concentration threshold at which the 2-mm probe becomes unreliable, as well as the overestimated sheet flow layer thickness.

Acknowledgments
The authors wish to thank the technical staff at LEGI (Stéphane Mercier, Jean-Marc Barnoud and Nicole Lambert) for their technical assistance during the experiments. This research was funded by the Région Rhône-Alpes (COOPERA project and Explora Pro grant), the French national program EC2CO-LEFE MODSED, the European Community's Horizon 2020 Program through the Integrated Infrastructure Initiative HYDRALAB+ COMPLEX (654110), and the French DGA funded ANR ASTRID Maturation project MESURE (ANR-16-ASMA-0005-01). Mieras and Puleo were supported by the National Science Foundation (grant 1356855) and the University of Delaware. This research was performed, in part, while Mieras held an NRC Research Associateship award at the U.S. Naval Research Laboratory. The data presented in this manuscript are available at Zenodo repository https://doi.org/10.5281/zenodo.1443459. Comments and remarks raised by the two anonymous reviewers helped to improve the quality of the paper.

References

Archie, G. E. (1942). The electrical resistivity log as an aid in determining some reservoir characteristics. *Transactions of AIME*, *146*(01), 54–62. https://doi.org/10.2118/942054-G

Armanini, A., Capart, H., Fraccarollo, L., & Larcher, M. (2005). Rheological stratification in experimental free-surface flows of granular-liquid mixtures. *Journal of Fluid Mechanics*, *532*, 269–319. https://doi.org/10.1017/S0022112005004283

Bagnold, R. A. (1956). The flow of cohesionless grains in fluids. *Philosophical Transactions. Royal Society of London*, *249*(964), 235–297. https://doi.org/10.1098/rsta.1956.0020

Berzi, D. (2011). Analytical solution of collisional sheet flows. *Journal of Hydraulic Engineering*, *137*(10), 1200–1207. https://doi.org/10.1061/(ASCE)HY.1943-7900.0000420

Bricault, M. (2006). Rétrodiffusion acoustique par une suspension en milieu turbulent: application à la mesure de profils de concentration pour l'étude de processus hydrosédimentaires. Grenoble, INPG.

Capart, H., & Fraccarollo, L. (2011). Transport layer structure in intense bed-load. *Geophysical Research Letters*, *38*, L20402. https://doi.org/10.1029/2011GL049408

Chassagneux, F. X., & Hurther, D. (2014). Wave bottom boundary layer processes below irregular surfzone breaking waves with light-weight sheet flow particle transport. *Journal of Geophysical Research: Oceans*, *119*, 1668–1690. https://doi.org/10.1002/2013JC009338

Chiodi, F., Claudin, P., & Andreotti, B. (2014). A two-phase flow model of sediment transport: Transition from bedload to suspended load. *Journal of Fluid Mechanics*, *755*, 561–581. https://doi.org/10.1017/jfm.2014.422

Cowen, E. A., Dudley, R. D., Liao, Q., Variano, E. A., & Liu, P. L.-F. (2010). An in situ borescopic quantitative imaging profiler for the measurement of high concentration sediment velocity. *Experiments in Fluids*, *49*(1), 77–88. https://doi.org/10.1007/s00348-009-0801-8

Daniel, S. M. (1965). *Flow of suspension in a rectangular channel*. Canada: University of Saskatchewan.

Horikawa, K., Watanabe, A., & Katori, S. (1982). Sediment transport under sheet flow condition. In *Coastal Engineering* (pp. 1335–1352).

Hsu, T. J., Jenkins, J. T., & Liu, L. F. (2003). On two-phase sediment transport: Dilute flow. *Journal of Geophysical Research*, *108*(C3), 3057. https://doi.org/10.1029/2001JC001276

Hurther, D., & Lemmin, U. (2001). Shear stress statistics and wall similarity analysis in turbulent boundary layers using a high resolution 3D ADVP. *Journal of Oceanic Engineering*, *25*, 446–457.

Hurther, D., & Lemmin, U. (2008). Improved turbulence profiling with field-adapted acoustic Doppler velocimeters using a bifrequency Doppler noise suppression method. *Journal of Atmospheric and Oceanic Technology*, *25*(3), 452–463. https://doi.org/10.1175/2007JTECHO512.1

Hurther, D., & Thorne, P. D. (2011). Suspension and near-bed load sediment transport processes above a migrating, sand-rippled bed under shoaling waves. *Journal of Geophysical Research*, *116*, C07001. https://doi.org/10.1029/2010JC006774

Hurther, D., Thorne, P. D., Bricault, M., Lemmin, U., & Barnoud, J.-M. (2011). A multi-frequency Acoustic Concentration and Velocity Profiler (ACVP) for boundary layer measurements of fine-scale flow and sediment transport processes. *Coastal Engineering*, *58*(7), 594–605. https://doi.org/10.1016/j.coastaleng.2011.01.006

Jackson, R. (1997). Locally averaged equations of motion for a mixture of identical spherical particles and a Newtonian fluid. *Chemical Engineering Science*, *52*(15), 2457–2469. https://doi.org/10.1016/S0009-2509(97)00065-1

Jenkins, J. T., & Hanes, D. M. (1998). Collisional sheet flows of sediment driven by a turbulent fluid. *Journal of Fluid Mechanics*, *370*, 29–52. https://doi.org/10.1017/S0022112098001840

Lanckriet, T., Puleo, J., Masselink, G., Turner, I., Conley, D., Blenkinsopp, C., & Russell, P. (2014). Comprehensive field study of swash-zone processes. II: Sheet flow sediment concentrations during quasi-steady-backwash. *Journal of Waterway, Port, Coastal, and Ocean Engineering*, *140*(1), 29–42. https://doi.org/10.1061/(ASCE)WW.1943-5460.0000209

Lanckriet, T., & Puleo, J. A. (2013). Near-bed turbulence dissipation measurements in the inner surf and swash zone. *Journal of Geophysical Research: Oceans*, *118*, 6634–6647. https://doi.org/10.1002/2013JC009251

Lanckriet, T., Puleo, J. A., & Waite, N. (2013). A conductivity concentration profiler for sheet flow sediment transport. *IEEE Journal of Oceanic Engineering*, *38*(1), 55–70. https://doi.org/10.1109/JOE.2012.2222791

Liu, D., Liu, X., Fu, X., & Wang, G. (2016). Quantification of the bed load effects on turbulent open-channel flows. *Journal of Geophysical Research: Earth Surface*, *121*, 767–789. https://doi.org/10.1002/2015JF003723

Mieras, R. S., Puleo, J. A., Anderson, D., Cox, D. T., & Hsu, T.-J. (2017). Large-scale experimental observations of sheet flow on a sandbar under skewed-asymmetric waves. *Journal of Geophysical Research: Oceans*, *122*, 5022–5045. https://doi.org/10.1002/2016JC012438

Naqshband, S., Ribberink, J. S., Hurther, D., Barraud, P.-A., & Hulscher, S. (2014). Experimental evidence for turbulent sediment flux constituting a large portion of the total sediment flux along migrating sand dunes. *Geophysical Research Letters*, *41*, 8870–8878. https://doi.org/10.1002/2014GL062322

Naqshband, S., Ribberink, J. S., Hurther, D., & Hulscher, S. (2014). Bed load and suspended load contributions to migrating sand dunes in equilibrium. *Journal of Geophysical Research: Earth Surface*, *119*, 1043–1063. https://doi.org/10.1002/2013JF003043

Nnadi, F. N., & Wilson, K. C. (1992). Motion of contact-load particles at high shear stress. *Journal of Hydraulic Engineering*, *118*(12), 1670–1684. https://doi.org/10.1061/(ASCE)0733-9429(1992)118:12(1670)

O'Donoghue, T., & Wright, S. (2004). Concentrations in oscillatory sheet flow for well sorted and graded sands. *Coastal Engineering*, *50*(3), 117–138. https://doi.org/10.1016/j.coastaleng.2003.09.004

Pugh, F. J., & Wilson, K. C. (1999). Velocity and concentration distributions in sheet flow above plane beds. *Journal of Hydraulic Engineering*, *125*(2), 117–125. https://doi.org/10.1061/(ASCE)0733-9429(1999)125:2(117)

Puleo, J. A., Blenkinsopp, C., Conley, D., Masselink, G., Turner, I. L., Russell, P., et al. (2014). Comprehensive field study of swash-zone processes. I: Experimental design with examples of hydrodynamic and sediment transport measurements. *Journal of Waterway, Port, Coastal, and Ocean Engineering*, *140*(1), 14–28.

Puleo, J. A., Lanckriet, T., Conley, D., & Foster, D. (2016). Sediment transport partitioning in the swash zone of a large-scale laboratory beach. *Coastal Engineering*, *113*, 73–87. https://doi.org/10.1016/j.coastaleng.2015.11.001

Revil-Baudard, T., & Chauchat, J. (2013). A two-phase model for sheet flow regime based on dense granular flow rheology. *Journal of Geophysical Research: Oceans*, *118*, 619–634. https://doi.org/10.1029/2012JC008306

Revil-Baudard, T., Chauchat, J., Hurther, D., & Barraud, P.-A. (2015). Investigation of sheet-flow processes based on novel acoustic high-resolution velocity and concentration measurements. *Journal of Fluid Mechanics*, *767*, 1–30. https://doi.org/10.1017/jfm.2015.23

Revil-Baudard, T., Chauchat, J., Hurther, D., & Eiff, O. (2016). Turbulence modifications induced by the bed mobility in intense sediment-laden flows. *Journal of Fluid Mechanics*, *808*, 469–484. https://doi.org/10.1017/jfm.2016.671

Ribberink, J. S., & Al-Salem, A. A. (1994). Sediment transport in oscillatory boundary layers in cases of rippled beds and sheet flow. *Journal of Geophysical Research*, *99*, 12,707–12,727. https://doi.org/10.1029/94JC00380

Ribberink, J. S., van der Werf, J. J., O'Donoghue, T., & Hassan, W. N. M. (2008). Sand motion induced by oscillatory flows: Sheet flow and vortex ripples. *Journal of Turbulence*, *9*. https://doi.org/10.1080/14685240802220009

Roelvink, J. A., & Brøker, I. (1993). Cross-shore profile models. *Coastal Engineering*, *21*(1–3), 163–191. https://doi.org/10.1016/0378-3839(93)90049-E

Spinewine, B., Capart, H., Fraccarollo, L., & Larcher, M. (2011). Laser stripe measurements of near-wall solid fraction in channel flows of liquid-granular mixtures. *Experiments in Fluids*, *50*(6), 1507–1525. https://doi.org/10.1007/s00348-010-1009-7

Sumer, B. M., Kozakiewicz, A., Fredsøe, J., & Deigaard, R. (1996). Velocity and concentration profiles in sheet-flow layer of movable bed. *Journal of Hydraulic Engineering*, *122*(10), 549–558. https://doi.org/10.1061/(ASCE)0733-9429(1996)122:10(549)

Thorne, P. D., & Campbell, S. C. (1992). Backscattering by a suspension of spheres. *Journal of Acoustical Society of America*, *92*(August), 978–986.

Thorne, P. D., & Hanes, D. M. (2002). A review of acoustic measurement of small-scale sediment processes. *Continental Shelf Research*, *22*(4), 603–632. https://doi.org/10.1016/S0278-4343(01)00101-7

Thorne, P. D., & Hurther, D. (2014). An overview on the use of backscattered sound for measuring suspended particle size and concentration profiles in non-cohesive inorganic sediment transport studies. *Continental Shelf Research*, *73*, 97–118. https://doi.org/10.1016/j.csr.2013.10.017

van der Zanden, J., Alsina, J. M., Cáceres, I., Buijsrogge, R. H., & Ribberink, J. S. (2015). Bed level motions and sheet flow processes in the swash zone: Observations with a new conductivity-based concentration measuring technique (CCM+). *Coastal Engineering*, *105*, 47–65. https://doi.org/10.1016/j.coastaleng.2015.08.009

van der Zanden, J., van Der A, D. A., Hurther, D., Caceres, I., O'Donoghue, T., Hulsher, S. J. M. H., & Ribberink, J. S. (2017). Bedload and suspended load contributions to breaker bar morphopdynamics. *Coastal Engineering*, *129*, 74–92.

Van Der Zanden, J., Van Der A, D. A., Hurther, D., Cáceres, I., O'Donoghue, T., & Ribberink, J. S. (2016). Near-bed hydrodynamics and turbulence below a large-scale plunging breaking wave over a mobile barred bed profile. *Journal of Geophysical Research: Oceans*, *121*, 6482–6506. https://doi.org/10.1002/2016JC011909

Wilson, G. W., & Hay, A. E. (2016). Acoustic observations of near-bed sediment concentration and flux statistics above migrating sand dunes. *Geophysical Research Letters*, *43*, 6304–6312. https://doi.org/10.1002/2016GL069579

Wilson, K. C. (1966). Bed-load transport at high shear stress. *Journal of the Hydraulics Division*, *HY6*(92), 49–59.